XIV International Conference on Computational Plasticity. Fundamentals and Applications
COMPLAS XIV
E. Oñate, D.R.J. Owen, D. Peric & M. Chiumenti (Eds)

A VARIATIONAL GROWTH APPROACH TO TOPOLOGY OPTIMIZATION

JUNKER P. *, JANTOS D. R.† and HACKL K.†

* Institute of Continuum Mechanics
Ruhr-Universität Bochum
Universitätsstraße 150, 44801 Bochum, Germany
e-mail: philipp.junker@rub.de

†Institute of Mechanics of Materials
Ruhr-Universität Bochum
Universitätsstraße 150, 44801 Bochum, Germany
e-mail: dustin.jantos@rub.de

Key words: Topology Optimization, Variational Growth, Regularization

Abstract. In this contribution we present an overview of our work on a novel approach to topology optimization based on growth processes [1, 2, 3]. A compliance parameter to describe the spatial distribution of mass is introduced. It serves as an internal variable for which an associated evolution equation is derived using Hamilton's principle. The well-known problem of checkerboarding is faced with energy regularization techniques. Numerical examples are given for demonstration purposes.

1 INTRODUCTION

The objective of topology optimization is to find the topology of a mechanical structure that possess maximum stiffness at minimum weight for given boundary conditions. The topology of a structure can be described by the spatial distribution of mass density within a design space Ω which is subject the boundary conditions i.e. loading and supports. The spatial distribution of mass density serves as indicator function for areas where material and no material (i.e. void) is located. We introduce a continuous interpolation between full material and void for the spatial distribution of density mass as $\rho(\boldsymbol{x}) \in [0,1] \; \forall \; \boldsymbol{x} \in \Omega$. With a non-linear interpolation for the material stiffness (or compliance), intermediate densities $\rho \in \,]0,1[$ can be penalized to provide solution containing only full material ($\rho = 1$) and void ($\rho = 0$). This principle is similar to the well-known SIMP (**S**olid **I**sotropic **M**aterial with **P**enalization) method [5]. According to Bendsøe [5], the problem of topology optimization for a linear-elastic material then reads

$$\min_{\mathbb{E} \in \mathcal{E}_{\text{ad}}} \min_{\boldsymbol{\sigma} \in \mathcal{S}} \left\{ \frac{1}{2} \int_{\Omega} \boldsymbol{\sigma} : \mathbb{C}(\boldsymbol{x}) : \boldsymbol{\sigma} \; \mathrm{d}V \right\} \tag{1}$$

$$\text{with} \qquad \mathcal{S} = \{ \boldsymbol{\sigma} \mid \nabla \cdot \boldsymbol{\sigma} + \boldsymbol{b} = \boldsymbol{0} \text{ in } \Omega, \; \boldsymbol{\sigma} \cdot \boldsymbol{n} = \boldsymbol{t} \text{ on } \partial_{\sigma} \Omega \}$$

where $\boldsymbol{\sigma}$ are the stresses, $\boldsymbol{b}$ are the body forces, and $\boldsymbol{t}$ are the given external tractions that act on the boundary $\partial_\sigma\Omega$. The interpolated material compliance is given by $\mathbb{C}(\boldsymbol{x}) = (\rho(\boldsymbol{x})\mathbb{E}_0)^{-1}$ with the full material stiffness $\mathbb{E}_0$. The set of admissible stiffness tensors $\mathcal{E}_{\text{ad}}$ can be defined in various ways, see [5].

In the proposed approach, we do not solve the problem of topology optimization in a strict way as demanded by Eq. (1). In contrast, we interpret that subject as a problem of optimized and *localized* growth of material. For this purpose, we introduce a compliance parameter (i.e. the inverse of the mass density ρ) which is the additional unknown at the material point (= integration point) level. The governing equations are determined using fundamental principles of thermodynamics which minimize the Gibbs energy. To account for a dissipative behavior, we apply Hamilton's principle. In this way, we are able to determine an evolution equation for the spatial distribution of density mass, which can be evaluated in an iterative update process within a solitary finite element environment like it is common in (microstructural) material modeling e.g. phase transformations, damage, and plasticity.

The evolution equation describes the pseudo-time dependent and local material growth for the current loading conditions. It hence predicts for each structure volume the single topology exhibiting maximum stiffness, depending on the time history. Surely, a completely filled design space Ω possesses per se maximum stiffness (which is equivalent to minimum compliance); however, it is not optimal regarding that only a minimum of mass shall be used. It is thus necessary to constraint the volume structure by either prescribe the total structure volume or model the continuous growth of the structure. In our work, we model the structure growth with two different approaches. Firstly, we introduce evolution equations with a visco-plastic ansatz providing a yield surface for the structure growth: the local density $\rho(\boldsymbol{x})$ only increases in areas where the stresses $\boldsymbol{\sigma}$ are higher than a specific threshold. Secondly, we combine a viscous ansatz for the evolution equation with a Lagrange multiplier which allows us to directly control the structure volume within time. With the *Lagrange shift* approach we define a special growth function which depends only on one parameter, but results in natural growth behavior.

An well-known phenomenon in SIMP-like approachs is the so called checkerboarding which become visible in the form of oscillating mass distributions (see Figure 1): spatial points that possess mass are directly neighbored to spatial points that are mass-free. This numerical artifact produces results that depend on the finite element mesh used for mathematical discretization and repeats (locally at the smallest discretization level) in a periodic manner. In the case of SIMP approaches, this phenomenon is present if tri-linear shape functions are used. In our case, comparable problems are observed which result from a non-convex Helmholtz free energy which is necessary to penalize the gray solution. We solve this problem with two different energy regularization approaches: on the one hand, we penalize the gradient of the spatial distribution of mass by introducing a field function which is coupled to the local compliance parameter. Penalizing the gradient of the field function thus penalizes also the spatial gradient of the compliance parameter. On the other hand, we directly penalize the gradient of the spatial distribution of mass. To condense the resulting field equation again to an evolution equation which can be evaluated *locally*,

we employ special shape functions for the balance equation of the compliance parameter using a discontinuous Galerkin approach.

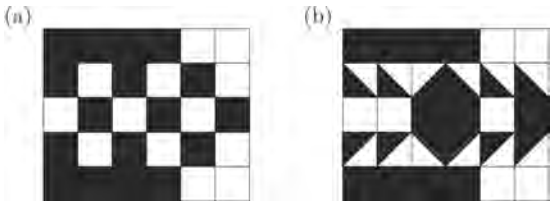

Figure 1: Schematic plot [2] of the usual inter-element checkerboarding (a) for approaches where the spatial distribution of mass is discretized element-wise, and (b) of the intra-element checkerboarding which was observed for our approach with the density field discretized within the integration points of each finite element. Whereas for "regular" checkerboarding entire elements are fluctuating between mass and no mass, mass fluctuates between zero and one *within* elements for the intra-element checkerboarding.

2 VARIATIONAL MODEL

2.1 Hamilton's principle

The Hamilton principle for dissipative continua reads

$$\delta\mathcal{G} + \int_\Omega \frac{\partial \mathcal{D}}{\partial \dot{\chi}} \delta\chi \, \mathrm{d}V + \delta\mathcal{P} = 0 \tag{2}$$

where $\mathcal{G}$ is the Gibbs energy, $\mathcal{D}$ is the dissipation function, χ is a internal variable to describe the spatial distribution of mass, and the functional $\mathcal{P}$ accounts for the problem-specific constraints. For linear elastic materials the Gibbs energy can be defined as

$$\mathcal{G} = \int_\Omega \Psi \, \mathrm{d}V - \int_\Omega \boldsymbol{b} \cdot \boldsymbol{u} \, \mathrm{d}V - \int_{\partial\Omega} \boldsymbol{t} \cdot \boldsymbol{u} \, \mathrm{d}A \tag{3}$$

with the Helmholtz energy

$$\Psi = \Psi_\mathrm{m} + \Psi_\mathrm{r} = \frac{1}{2} \int_\Omega \boldsymbol{\sigma} : \mathbb{C}(\boldsymbol{x}) : \boldsymbol{\sigma} \, \mathrm{d}V + \Psi_\mathrm{r} \tag{4}$$

composed of the part for the regularization Ψ_r and the mechanical part Ψ_m containing the constitutive law with $\boldsymbol{\sigma} = (\mathbb{C}^{-1}(\boldsymbol{x})) : \boldsymbol{\varepsilon}$ and the strains $\boldsymbol{\varepsilon} = \frac{1}{2}(\nabla\boldsymbol{u} + \boldsymbol{u}\nabla)$ containing the displacement field $\boldsymbol{u}$. As we can see here, by minimizing the Gibbs energy $\mathcal{G}$ we also find the minimum of the Helmholtz energy which solves the minimization problem in Eq. (1). We introduce the compliance parameter $\chi(\boldsymbol{x}) \in [0, 1]$ as internal variable to describe the spatial distribution of mass with $\chi = 0 \rightarrow$ full material and $\chi = 1 \rightarrow$ void. As stated before, we apply a non-linear interpolation for the material compliance penalizing intermediate solutions $\chi \in]0, 1[$

$$\mathbb{C}(\chi) = \chi^2 \, \mathbb{C}_\mathrm{void} + (1 - \chi^2)\mathbb{C}_0 \tag{5}$$

For numerical reasons, the material stiffness of the void material cannot be zero. Thus, the material compliance of the void $\mathbb{C}_\mathrm{void}$ must be finite but much larger than the full

material compliance $\mathbb{C}_0$. We introduce the small but non-zero numerical parameter κ and define $\mathbb{C}_{\text{void}} = \frac{1}{\kappa}\,\mathbb{C}_0$ which yields

$$\mathbb{C}(\chi) = f(\chi)\mathbb{C}_0 \quad \Leftrightarrow \quad \mathbb{E}(\chi) = \frac{1}{f(\chi)}\mathbb{E}_0 \tag{6}$$

with the interpolation function $f(\chi)$, which is the inverse of our density function $\rho(\boldsymbol{x})$ (due to numerical reasons the domain for the density function becomes $\rho(\boldsymbol{x}) \in [\kappa, 1]$).

$$f(\chi) = \frac{1}{\rho(\chi)} = 1 + \left(\frac{1}{\kappa} - 1\right)\chi^2 \tag{7}$$

We define the constraint functional $\mathcal{P}$ as

$$\mathcal{P} := \int_\Omega \gamma\,\chi \;\mathrm{d}V \tag{8}$$

with the Kuhn-Tucker parameter γ which constrains the interval of the internal variable $\chi \in [0, 1]$. The Dissipation function $\mathcal{D}$ and the regularization part of the Helmholtz energy Ψ_r vary for the different approaches and will be presented in the following section.

The Gibbs energy constitutes as functional depending on the displacement field $\boldsymbol{u}(\boldsymbol{x})$ and the spatial distribution of the internal variables $\chi(\boldsymbol{x})$, which are also the unknowns for the optimization problem. Thus, the variation in Eq. (2) has to be performed for $\boldsymbol{u}$ and χ which can be evaluated independently. The variation with respect to the displacement field $\boldsymbol{u}$ yields the well-known the balance of linear momentum in its weak form

$$\delta_{\boldsymbol{u}}\mathcal{G} = \int_\Omega \frac{\partial \Psi_\mathrm{m}}{\partial \boldsymbol{\varepsilon}} : \delta\boldsymbol{\varepsilon} \;\mathrm{d}V - \int_\Omega \boldsymbol{b}\cdot\delta\boldsymbol{u} \;\mathrm{d}V - \int_{\partial\Omega} \boldsymbol{t}\cdot\delta\boldsymbol{u} \;\mathrm{d}A = 0 \qquad \forall\,\delta\boldsymbol{u} \tag{9}$$

which can be solved with a common finite element method. The variation with respect to the internal variable χ yields the evolution equation for the compliance parameter in the form $\dot{\chi} = \mathrm{func}(\boldsymbol{\sigma}, \boldsymbol{\varepsilon}, \chi, ...)$. With the results from the finite element method, the evolution equation can be evaluated in an explicit manner after each iteration step i as

$$\chi^{(i+1)} = \chi^{(i)} + \Delta t \dot{\chi}(\boldsymbol{\sigma}^{(i)}) \tag{10}$$

which closes the system of equations to solve the optimization problem. The whole procedure can be incorporated in a Newton-Raphson iteration as done in e.g. damage and plasticity modeling. The actual form of the evolution equation vary for the different approaches shown in the following sections. However, all approaches share the same (mechanical) driving force

$$p_\chi := -\frac{\partial \Psi_\mathrm{m}}{\partial \chi} = -\frac{1}{2}\,\boldsymbol{\sigma} : f'(\chi)\mathbb{C}_0 : \boldsymbol{\sigma} \tag{11}$$

2.2 Regularization of a field function

In our first appraoch [1], we chose a dissipation function $\mathcal{D}$ which yields an evolution equation of elasto-viscoplatic type, as

$$\mathcal{D} = r_1|\dot{\chi}| + r_2\,\frac{\dot{\chi}^2}{2} \quad \Rightarrow \quad \frac{\partial \mathcal{D}}{\partial \dot{\chi}} = r_1\,\partial|\dot{\chi}| + r_2\,\dot{\chi} \tag{12}$$

with the subdifferential $\partial|\dot{\chi}|$ reading

$$\partial|\dot{\chi}| = \begin{cases} \{|\dot{\chi}| \leq 1\} & \text{for } \dot{\chi} = 0 \\ \dfrac{\dot{\chi}}{|\dot{\chi}|} & \text{else} \end{cases} \tag{13}$$

We apply the method of gradient-enhanced free energy for the regularization.The energy Ψ_r contains two term: the first one couples the local information carried by χ to a field function $\varphi(\boldsymbol{x})$. The second term penalizes "large" gradients of φ. We define the regularization part of the Helmholtz energy Ψ_r as

$$\Psi_\mathrm{r} = \frac{\alpha}{2}|\nabla\varphi|^2 + \frac{\beta}{2}(\varphi - \chi)^2 \tag{14}$$

Since χ is coupled to φ, penalization of the gradient of φ also influences the gradient of χ: "large" gradients of χ will be penalized. Because the oscillating pattern of checkerboarding possess "large" gradients of χ, checkerboarding is energetically less favorable and will be suppressed. The slip between the compliance parameter and the field function holds the advantage that local evolution and the far-field behavior of χ can be controlled individually so that the width of the transition zone can be adjusted. This advantage is accompanied by the drawback of a highly increased numerical effort due to the increased number of nodal unknowns.

The variation of Eq. (2) with respect to the internal variable χ yields the evolution equation

$$\dot{\chi} = \frac{1}{r_2}\big[|p_\chi + \beta(\varphi - \chi)| - r_1\big]_+ \,\mathrm{sgn}(p_\chi + \beta(\varphi - \chi)) \tag{15}$$

where $\big[x\big]_+ := (x + |x|)/2$ implies that only positive values are taken into account to ensure structure growth. The the sgn-function reads

$$\mathrm{sgn}p = \begin{cases} 1 & \text{for } p > 0 \\ -1 & \text{for } p < 0 \\ \{\tilde{p} \leq 1\} & \text{for } p = 0 \end{cases} \tag{16}$$

In addition, we have to calculate the variation of Eq. (2) with respect to the field function φ, which yields

$$\int_\Omega \beta\ (\varphi - \chi)\ \delta\varphi\ \mathrm{d}V + \int_\Omega \alpha\ \nabla\varphi\ \nabla\delta\varphi\ \mathrm{d}V = 0 \tag{17}$$

Eqs. (17) and (9) can be solved with the finite element method where the field function φ can be discretized with common shape-functions and becomes an additional nodal unknown (besides the 3 degrees of freedom of the displacement field) for the Newton-Raphson scheme.

2.3 Regularization by direct gradient penalization

In our second approach [2], we penalize the gradient of the internal variable χ directly without introducing a field function φ by applying the energy

$$\Psi_{\mathrm{r}} = \frac{\alpha}{2}|\nabla\chi|^2 \tag{18}$$

The variation of the Gibbs energy with respect to the internal variable χ yields a condition similar to Eq. (17). Instead of using this equation to add the internal variable χ as additional nodal degree of freedom as done for φ, we approximate the gradient of the internal variable with a discontinous Galerkin approach. The tri-linear discontinuous shape functions $\boldsymbol{N}_\chi$ discretize values for the internal variable within the Gauß (integration) points of the finite element mesh. Thus, the gradient of the internal variable will be evaluated *within* each finite element. As shown in Figure 1, checkerboarding occurs in an intra-element way in our approach. Therefore we do not need any penalization of the gradient "over element borders" to suppress checkerboarding. We apply the same dissipation function $\mathcal{D}$ given in Eq. (12) and find the evolution equation

$$\dot{\chi} = \frac{1}{r_2}\left[|p - \overline{\Delta\chi}| - r_1\right]_+ \ \mathrm{sgn}\left[p - \overline{\Delta\chi}\right] \tag{19}$$

with

$$\overline{\Delta\chi_i} := \frac{1}{|\Omega_{\mathrm{e}}|}\left(\int_{\Omega_{\mathrm{e}}} \alpha\,(\nabla\boldsymbol{N}_\chi)^T \cdot (\nabla\boldsymbol{N}_\chi \cdot \tilde{\boldsymbol{\chi}})\ \mathrm{d}V\right)_i \tag{20}$$

where the index refers to a local evaluation at the Gauß (integration) points in each element ($\boldsymbol{x}_{\mathrm{GP},i,\mathrm{e}}$) with volume $|\Omega_{\mathrm{e}}|$. Except for the integral in $\overline{\Delta\chi_i}$, equation (14) can be completely evaluated locally at the Gauß (integration) points as done in e.g. plasticity: the internal variable χ can be evaluated locally without monolithically solution for the whole finite element mesh. The quantity $\overline{\Delta\chi_i}$ is the only one which also depends on other $\chi_k, k \neq i$: the compliance parameters enter $\nabla\boldsymbol{N}_\chi\cdot\tilde{\boldsymbol{\chi}}$ for all Gauß (integration) points in the single element in which χ_i is located. Hence, $\overline{\Delta\chi_i}$ is a measure for the gradient within each element and thus ensures the gradient-penalization which regularizes the Gibbs energy and suppresses the intra-element checkerboarding.

2.4 Controlled growth

In [3], we introduce a Lagrange multiplier to directly control the structure volume within the iteration process. The Lagrange multiplier prevents the trivial solution and therefore the plasticity part in the Dissipation function is not needed anymore. We define

$$\mathcal{D} = r_2\,\frac{\dot{\chi}^2}{2} \tag{21}$$

and the constraint for controlled growth

$$g(\chi) = \frac{1}{|\Omega|}\int_\Omega \rho(\chi)\ \mathrm{d}V - \varrho(t) = \frac{1}{|\Omega|}\int_\Omega \frac{1}{f(\chi)}\ \mathrm{d}V - \varrho(t) \stackrel{!}{=} 0 \tag{22}$$

where $\varrho(t)$ denotes a prescribed growth function. To incorporate this constraint, we have to expand the constraint functional $\mathcal{P}$ as

$$\mathcal{P} := g(\chi) + \int_\Omega \gamma\, \chi \, \mathrm{d}V \tag{23}$$

We apply the regularization scheme including the discontinuous Galerkin approach given in the previous section. The final evolution equation reads

$$\dot{\chi} = \frac{1}{r_2} \left[\frac{\lambda}{|\Omega|} \frac{f'(\chi)}{f(\chi)^2} + p_\chi - \frac{\overline{\Delta\chi}}{|\Omega_\mathrm{e}|} \right] \tag{24}$$

with the Lagrange multiplier

$$\lambda = |\Omega| \, \frac{\displaystyle\int_\Omega \left(-p_\chi + \frac{\overline{\Delta\chi}}{|\Omega|_\mathrm{e}} \right) \frac{f'(\chi)}{f(\chi)^2} \, \mathrm{d}V - r_2 \, |\Omega| \, \dot{\varrho}(t)}{\displaystyle\int_\Omega \left(\frac{f'(\chi)}{f(\chi)^2} \right)^2 \mathrm{d}V} \tag{25}$$

Any arbitrary growth (discretized) function $\varrho(t^{(i)})$ can be inserted into the Lagrange multiplier in Eq. (25) as

$$\dot{\varrho}\left(t^{(i+1)}\right) = \frac{|\Omega| \; \varrho\left(t^{(i+1)}\right) - \displaystyle\int_\Omega \rho(\chi) \, \mathrm{d}V}{\Delta t} \tag{26}$$

For the growth function, we introduced the *Lagrange shift* approach with

$$\varrho(t) := \frac{1 - \lambda_\mathrm{S}}{V_\Omega} \int_\Omega \frac{1}{f\left(\chi(t)\right)} \, \mathrm{d}V \bigg|_{\lambda=0} \tag{27}$$

where $0 < \lambda_\mathrm{S} < 1$ is a numerical parameter. For the Lagrange multiplier follows

$$\lambda = \lambda_\mathrm{S} \; V_\Omega \, \frac{\displaystyle\int_\Omega \left(-p_\chi + \frac{\overline{\Delta\chi}}{V_\mathrm{e}} + \gamma \right) \frac{f'(\chi)}{f(\chi)^2} \, \mathrm{d}V}{\displaystyle\int_\Omega \left(\frac{f'(\chi)}{f(\chi)^2} \right)^2 \mathrm{d}V} \tag{28}$$

The parameter λ_S shifts the model behavior between two "extreme cases": if $\lambda_\mathrm{S} = 1$, there is no growth and the model preserves the structure volume. Choosing $\lambda_\mathrm{S} = 0$ would lead to a model without any restrictions for the structure growth which would obviously result in the trivial solution since the density would increase simultaneously in the entire design space. The *Lagrange shift* approach is numerically quite stable and leads to natural growth behavior. The benefit of the *Lagrange shift* approach is that only one bounded parameter $\lambda_\mathrm{S} \in]0, 1[$ must be chosen to define the growth function. If the solution for a given structure volume is desired, the growth function can be switched according to Eq. (26) (with $\varrho\left(t^{(i+1)}\right) = \text{const.}$ as the target volume) as soon as the structure volume exceeds the given target volume.

3 NUMERICAL RESULTS

Let us now present some numerical results for the three different approaches. Our first example is a simply supported beam given in Figure 2. The essential process of the evolution of the structure is similar for all approaches given in [1, 2, 3]. Figure 2 shows the results for the model given in [3] representative for all models. The model given in [3] differs from the other models in one point: this model allows us to hold the structure volume constant for additional iteration steps, in which the structure is further optimized so that the structural stiffness ($\mathcal{S} = 1/\hat{\boldsymbol{f}} \cdot \hat{\boldsymbol{u}}$) is increased for the same structure volume (see Figure 3). In contrast, the results from the other two approaches are just snapshots for structures with the respective volume structure while the model leads to a continuous growth towards the trivial solution of a structure volume that equals the design space. A comparison of the final results from all approaches for a structure volume $\varrho = 45.65\%$ are given in Figure 3 and 3. The difference between Firgure 3 and 3 is the fineness of the finite element mesh to show the mesh-independence of our models.

As a second example, we introduce a three-dimensional bending problem. The boundary conditions and final results for each model are given in Figure 3.

4 CONCLUSIONS

We presented a novel approach to topology optimization based on the thermodynamic principles known from variational material modeling. The numerical results of all approaches showed overall fine, smooth and reasonable structures, although relatively coarse meshes were used. Checkerboarding was suppressed by energy regularization with two different approaches. The regularization by aid of a field function in [1] holds the advantage that the transition zone between material and void phase can be controlled independently from the actual regularization. This is not possible with the direct gradient penalization of the internal variable in [2]. However, the approach in [2] does not need to introduce additional nodal degrees of freedom by using a discontinuous Galerkin discretization for the internal variable. This reduces the calculation effort remarkably ($\approx 10\%$ of [1]). In [3], we added a way to directly control the structure mass by aid of a Lagrange multiplier which allows us mimic natural growth and find further optimized structures for given structure volumes. The *Lagrange shift* approach led to easy-to-handle and numerically stable growth.

The usage of a variational approach based on thermodynamic principles holds the advantage that the general experience and research results in material modeling (e.g. from phase transformation and plasticity modeling) can be accounted for the development of topology optimization approaches. For example, additional design characteristics for the structure (e.g. the material orientation for anisotropic materials [4]) can be incorporated as additional design variables. Due to the growth-based approaches we are using a close link also to biological systems seems feasible and will be subject of future investigations.

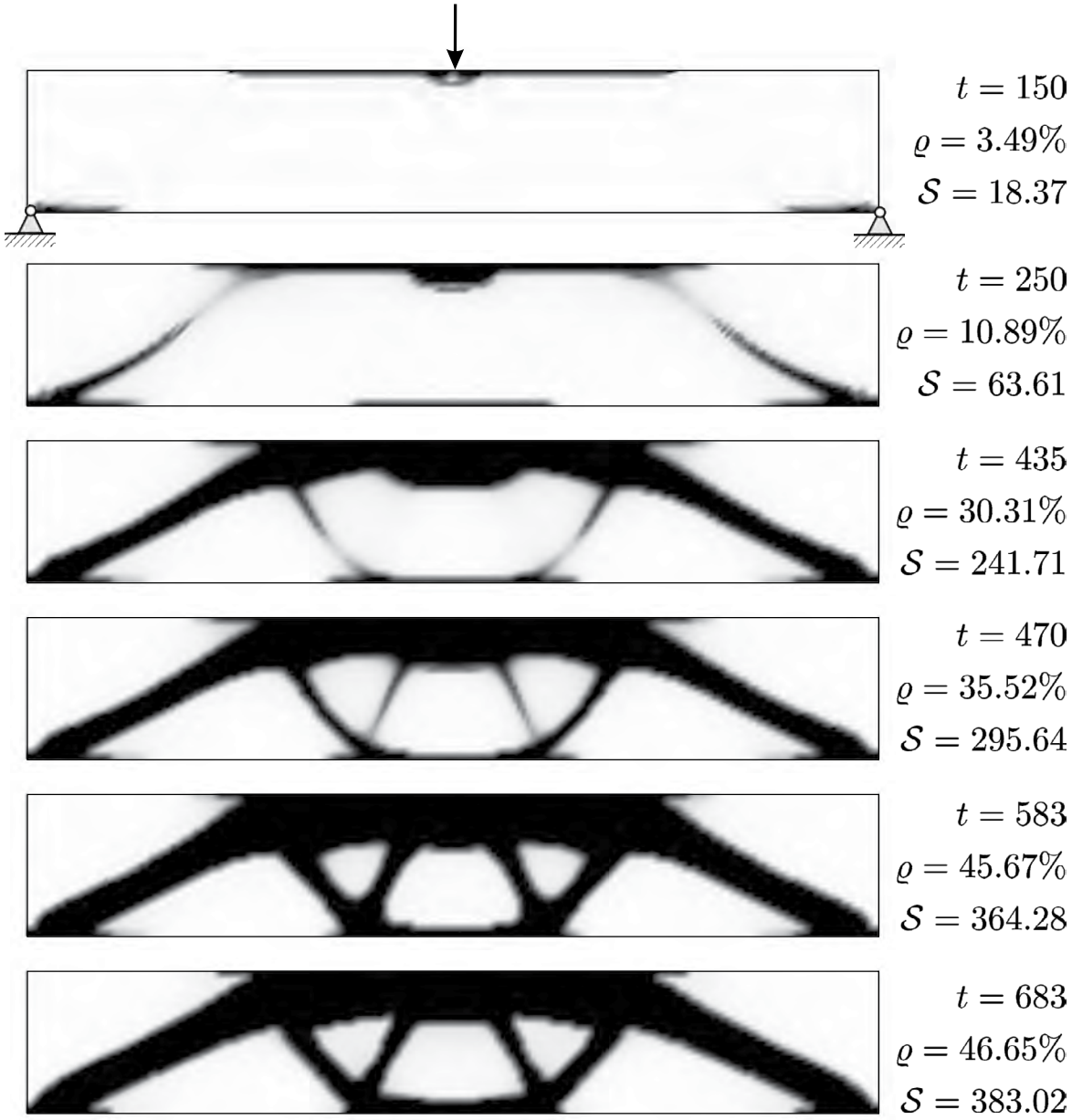

Figure 2: Resulting structural evolution from the model given in 2.4. As soon as the structure volume of $\varrho = 45.65\%$ is reached, the structure volume is held constant for additional 100 iteration steps according to Eq. (26)

REFERENCES

[1] Junker, P. and Hackl, K. *A variational growth approach to topology optimization.* Structural and Multidisciplinary Optimization, Vol. 300,p. 780-801, (2015).

[2] Junker, P. and Hackl, K. *A discontinuous phase field approach to variational topology optimization.* Structural and Multidisciplinary Optimization, Vol. 52, pp. 293-304,

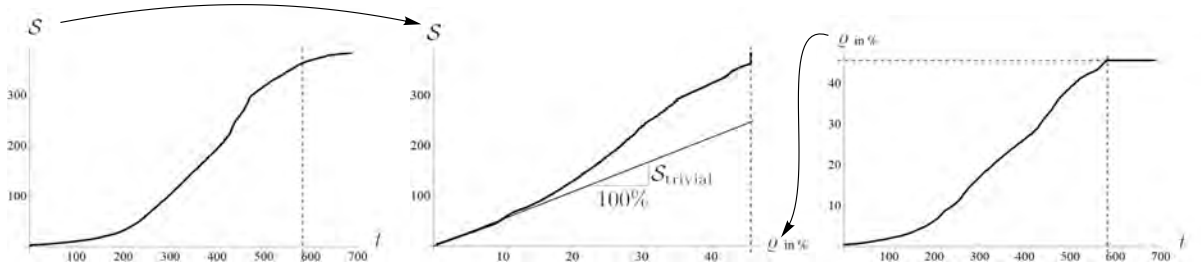

Figure 3: Structure stiffness $\mathcal{S}$ within simulation process, structure stiffness with respect to structure volume ϱ, and structure volume $\mathcal{S}$ within simulation process (from the left hand to the right hand side). The dashed gray lines mark the iteration step $t = 582$ and the structure volume $\varrho = 45.65\%$ which is held constant at this value for iteration steps $t > 582$. The line in the upper right picture shows the linear interpolation of the Stiffness for the trivial solution $\mathcal{S}_{\text{trivial}} = \mathcal{S}(\chi(\boldsymbol{x}) = 0)\ \forall\ \boldsymbol{x} \in \Omega$ over the structure volume ϱ.

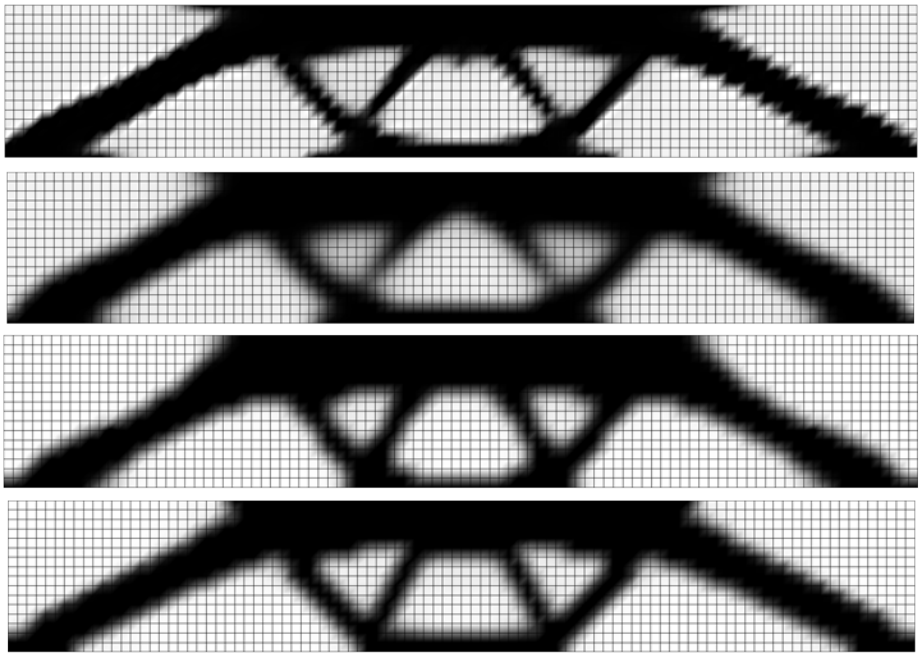

Figure 4: Results for a mesh with $144 \times 96 \times 1$ cubic elements on 3298 nodes from top to bottom: model in [1] (Section 2.2), model in [2] (Section 2.3), model in [3] (Section 2.4) as soon as $\varrho = 45.65\%$ and after additional 100 iteration steps.

(2015).

[3] Jantos, D. R. and Junker, P. and Hackl, K. *An evolutionary topology optimization approach with variationally controlled growth*. Computer Methods in Applied Mechanics and Engineering, Vol. 300,p. 780-801, (2016).

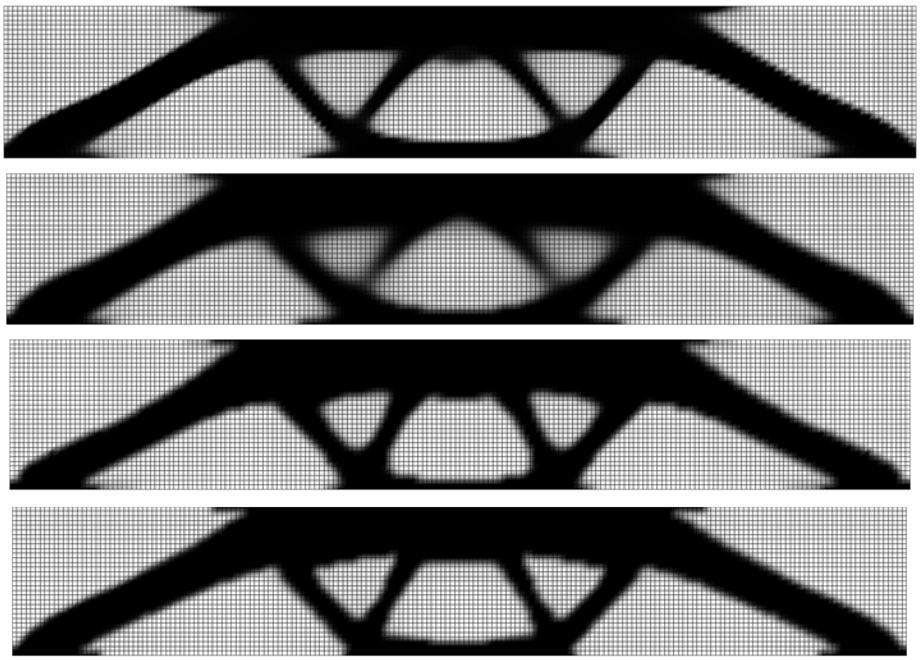

Figure 5: Results for a mesh with $192 \times 32 \times 1$ cubic elements on 12738 nodes from top to bottom: model in [1] (Section 2.2), model in [2] (Section 2.3), model in [3] (Section 2.4) as soon as $\varrho = 45.65\%$ and after additional 100 iteration steps.

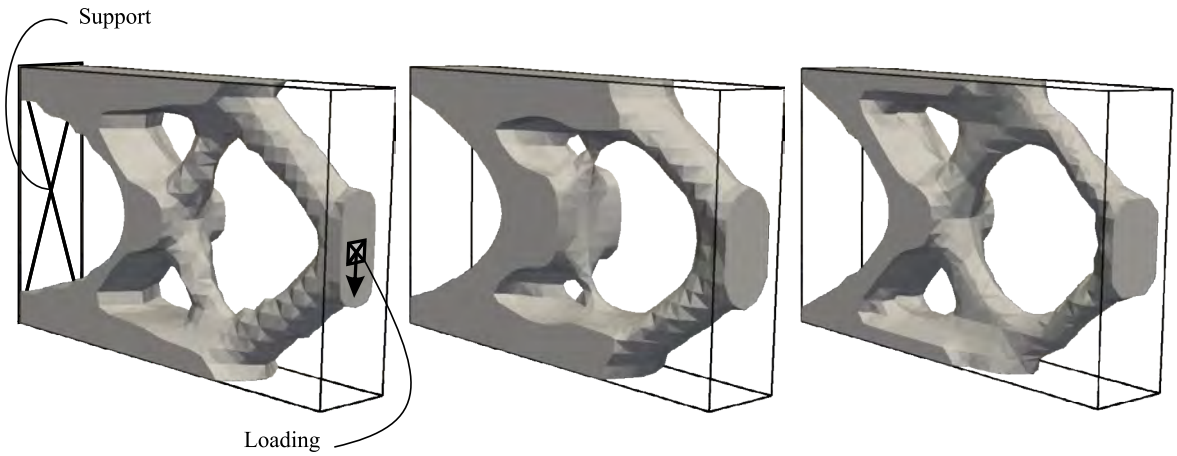

Figure 6: From left to right: Boundary conditions, results for the model in [1] (Section 2.2), model in [2] (Section 2.3), and model in [3] (Section 2.4). Discretization: $32 \times 20 \times 6$ cubic elements on 4851 node. Structure volume: $\varrho = 30\%$.

[4] Jantos, D. R. and Junker, P. and Hackl, K. *Optimized growth and reorientation of anisotropic material based on evolution equations*. Submitted

[5] Bendsøe, M. P. and Sigmund, O *Topology optimization: theory, methods and appli-*

cations. Springer (2003).